



## Discover Generics

Cost-Effective CT & MRI Contrast Agents

**FRESENIUS  
KABI**

[WATCH VIDEO](#)

# AJNR

This information is current as  
of June 23, 2025.

## **Novel Models for Identification of the Ruptured Aneurysm in Patients with Subarachnoid Hemorrhage with Multiple Aneurysms**












H. Rajabzadeh-Oghaz, J. Wang, N. Varble, S.-I. Sugiyama,  
A. Shimizu, L. Jing, J. Liu, X. Yang, A.H. Siddiqui, J.M.  
Davies and H. Meng

*AJNR Am J Neuroradiol* 2019, 40 (11) 1939-1946

doi: <https://doi.org/10.3174/ajnr.A6259>

<http://www.ajnr.org/content/40/11/1939>

# Novel Models for Identification of the Ruptured Aneurysm in Patients with Subarachnoid Hemorrhage with Multiple Aneurysms

 H. Rajabzadeh-Oghaz,  J. Wang,  N. Varble,  S.-I. Sugiyama,  A. Shimizu,  L. Jing,  J. Liu,  X. Yang,  A.H. Siddiqui,  J.M. Davies, and  H. Meng



## ABSTRACT

**BACKGROUND AND PURPOSE:** In patients with SAH with multiple intracranial aneurysms, often the hemorrhage pattern does not indicate the rupture source. Angiographic findings (intracranial aneurysm size and shape) could help but may not be reliable. Our purpose was to test whether existing parameters could identify the ruptured intracranial aneurysm in patients with multiple intracranial aneurysms and whether composite predictive models could improve the identification.

**MATERIALS AND METHODS:** We retrospectively collected angiographic and medical records of 93 patients with SAH with at least 2 intracranial aneurysms (total of 206 saccular intracranial aneurysms, 93 ruptured), in which the ruptured intracranial aneurysm was confirmed through surgery or definitive hemorrhage patterns. We calculated 13 morphologic and 10 hemodynamic parameters along with location and type (sidewall/bifurcation) and tested their ability to identify rupture in the 93 patients. To build predictive models, we randomly assigned 70 patients to training and 23 to holdout testing cohorts. Using a linear regression model with a customized cost function and 10-fold cross-validation, we trained 2 rupture identification models: RIM<sub>C</sub> using all parameters and RIM<sub>M</sub> excluding hemodynamics.

**RESULTS:** The 25 study parameters had vastly different positive predictive values (31%–87%) for identifying rupture, the highest being size ratio at 87%. RIM<sub>C</sub> incorporated size ratio, undulation index, relative residence time, and type; RIM<sub>M</sub> had only size ratio, undulation index, and type. During cross-validation, positive predictive values for size ratio, RIM<sub>M</sub>, and RIM<sub>C</sub> were 86% ± 4%, 90% ± 4%, and 93% ± 4%, respectively. In testing, size ratio and RIM<sub>M</sub> had positive predictive values of 85%, while RIM<sub>C</sub> had 92%.

**CONCLUSIONS:** Size ratio was the best individual factor for identifying the ruptured aneurysm; however, RIM<sub>C</sub>, followed by RIM<sub>M</sub>, outperformed existing parameters.

**ABBREVIATIONS:** AR = aspect ratio; CFD = computational fluid dynamics; D = maximum diameter; H = height (perpendicular); H<sub>max</sub> = maximum height; IA = intracranial aneurysm; NWSS = normalized wall shear stress; OSI = oscillatory shear index; RIM = rupture identification model; RRS = rupture resemblance score; RRT = relative residence time; SR = size ratio; UI = undulation index; WSS = wall shear stress

Approximately 30% of patients with intracranial aneurysms (IAs) present with multiple aneurysms.<sup>1</sup> Correct identifica-

tion of the ruptured IA in a patient with SAH is critical for treatment planning.<sup>2</sup> Identifying the ruptured IA is increasingly important in an era of increased endovascular treatment because the source of hemorrhage cannot be confirmed visually and aneurysms are usually treated individually. Hemorrhage pattern on initial CT scans is the primary indicator of the bleeding source, as demonstrated by Orning et al,<sup>3</sup> who reported that a definitive hemorrhage pattern (localized to 1 IA) could accurately delineate the ruptured IAs. However, in approximately half of patients with multiple aneurysms, the hemorrhage pattern cannot

Received December 5, 2018; accepted after revision August 23, 2019.


From the Canon Stroke and Vascular Research Center (H.R.-O., N.V., A.H.S., J.M.D., H.M.) and Departments of Mechanical and Aerospace Engineering (H.R.-O., N.V., H.M.) and Biostatistics (J.W.), University at Buffalo, Buffalo, New York; Department of Neuroanesthesia (S.-I.S.), Kohnan Hospital, Sendai, Japan; Department of Neurosurgery (S.-I.S., A.S.), Tohoku University Graduate School of Medicine, Sendai, Japan; Department of Interventional Neuroradiology (L.J., J.L., X.Y., H.M.), Beijing Neurosurgical Institute, Beijing Tiantan Hospital, Capital Medical University, Beijing, China; Departments of Neurosurgery (A.H.S., J.M.D.), Bioinformatics (J.M.D.), and Radiology (A.H.S.), Jacobs School of Medicine and Biomedical Sciences, University at Buffalo, Buffalo, New York; and Jacobs Institute (A.H.S., J.M.D.), Buffalo, New York.

This work was supported by National Institutes of Health grants R01NS091075 and R03NS090193 and Canon Medical Systems. J.M. Davies was supported by the National Center for Advancing Translational Sciences of the National Institutes of Health (award KL2TR001413 to the University at Buffalo). This work is also supported by National Key Research and Development Plan of China (grant 2016YFC1300800), the National Natural Science Foundation of China (grants 81220108007, 81371315, 81471167, and 81671139), and the Special Research Project for Capital Health Development (grant 2018-4-1077).

Please address correspondence to Hui Meng, PhD, Canon Stroke and Vascular Research Center, Clinical Translational Research Center, 875 Ellicott St, Buffalo, NY 14203; e-mail: huimeng@buffalo.edu

 Indicates open access to non-subscribers at [www.ajnr.org](http://www.ajnr.org)

 Indicates article with supplemental on-line appendix and tables.

 Indicates article with supplemental on-line photos.

<http://dx.doi.org/10.3174/ajnr.A6259>

delineate the ruptured IA.<sup>3</sup> In such cases, rupture identification relies on angiographic findings, such as IA size, shape, and location.<sup>2,3</sup> Several studies have reported misidentification of the ruptured aneurysm, which has been attributed to the small size or benign shape of the ruptured IA.<sup>2-8</sup> Therefore, developing more reliable means of identifying the ruptured IA has clinical value in patients with multiple IAs, especially when the hemorrhage pattern cannot delineate the ruptured IA.

Several morphologic and hemodynamic parameters have been found to differ significantly between ruptured and unruptured aneurysm cohorts in patients with multiple IAs, albeit with conflicting findings.<sup>9-15</sup> These studies have generally relied on univariate and multivariate regression analyses of pooled data of ruptured and unruptured IAs. Although such methods model the general probability of aneurysm rupture, they are not tailored for identifying which aneurysm ruptured in patients with SAH with multiple aneurysms. To that end, the ability of aneurysmal metrics for identification of the ruptured aneurysm should be evaluated by comparing all IAs within each patient, and models trained by associating the coexisting IAs within each patient should be developed.

In this study, we retrospectively analyzed IAs in patients with SAH presenting with multiple aneurysms to test the performance of existing morphologic and hemodynamic parameters and to build new composite models for identifying the ruptured aneurysm in patients with multiple aneurysms. The performance of the new models was compared against existing morphologic and hemodynamic parameters along with aneurysm location and type (sidewall or bifurcation) and a previously developed rupture-classification model, the rupture resemblance score (RRS).<sup>16</sup> Our findings may assist clinicians in better identifying the ruptured IA in patients with SAH presenting with multiple aneurysms.

## MATERIALS AND METHODS

### Ethics Approval

This study was approved by the institutional review board of the University at Buffalo (IRB: 30–510704: Virtual Intervention of Intracranial Aneurysms).

### Data Collection

We retrospectively collected cerebrovascular images and medical records from consecutive series of patients with aneurysmal SAH treated at 3 stroke centers located in China (Beijing Tiantan Hospital, Capital Medical University, Beijing, China), Japan (Kohnan Hospital, Sendai, Japan), and the United States (Gates Vascular Institute, Buffalo, NY). Inclusion criteria mandated that patients had a ruptured IA and at least 1 unruptured aneurysm and that all aneurysms were saccular. For the patients who underwent a craniotomy for aneurysm clipping, the ruptured aneurysm was confirmed through microscopic visual assessment. For patients who underwent endovascular or no treatment, we included only those with a definitive hemorrhage pattern on CT (localized to 1 IA). Examples of definitive and nondefinitive hemorrhage patterns are provided in Fig 1, respectively. All patients included in the current study underwent 3D rotational DSA preoperatively, which was used for

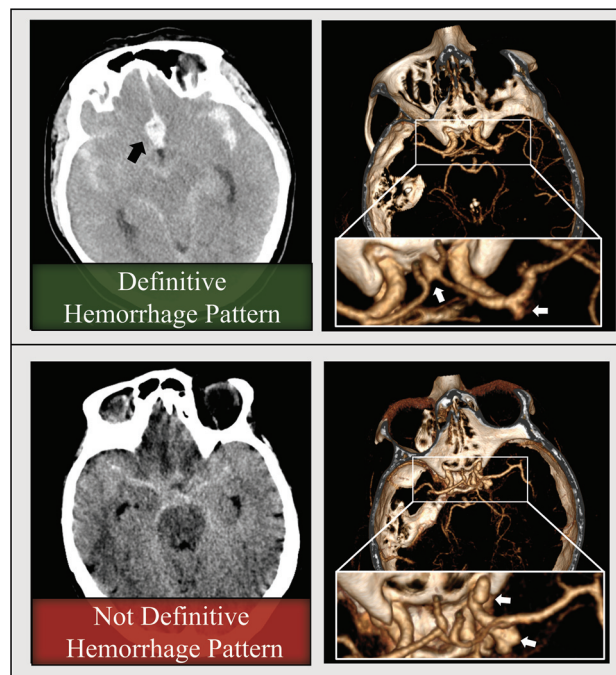


**FIG 1.** Top, A 62-year-old woman who presented with SAH (left image, noncontrast CT scan) was found to have anterior communicating artery and MCA aneurysms (white arrows, right image, CTA). A focal hematoma in the anterior circulation (black arrow, left image) delineated the anterior communicating artery aneurysm as the source of bleeding, which was confirmed at surgery. Bottom, A 59-year-old woman presented with SAH (left image, noncontrast CT scan). She was found to have 2 large lobulated right ICA aneurysms (white arrows, right image, CTA). The source of the rupture could not be identified from the hemorrhage pattern (this patient was excluded from our study). Both aneurysms were treated endovascularly.

aneurysm-geometry reconstruction. In general, the voxel sizes of images obtained at the 3 centers were similar, with little variation during the acquisition period: Chinese center, 0.280 mm; Japanese center, 0.227–0.226 mm; and US center, 0.256–0.223 mm. The images and data were anonymized, and the study received institutional review board approval. The operators who conducted image segmentation and morphologic and hemodynamic evaluations were blinded to aneurysm rupture status.

### Image Segmentation and Computational Fluid Dynamics

The 3D-DSA images of all patients were segmented using an open-source Vascular Modeling Toolkit (VMTK; <http://www.vmtk.org>). VMTK is a semiautomated tool that uses a level-set method to place lumen contours at regions with maximum gradient intensity.<sup>17</sup> After segmentation, a surface mesh for IAs with surrounding parent vessels was generated using the threshold-based marching cubes algorithm.<sup>17</sup>

Computational fluid dynamics (CFD) simulations were performed at 2 different centers (China: Beijing Tiantan Hospital, Capital Medical University, Beijing, China and Gates Vascular Institute, Buffalo, NY). For the Chinese data base, CFD was performed using ICEM-CFD software (ANSYS, Canonsburg, Pennsylvania) for mesh generation and CFX 14.0 software (ANSYS) for CFD simulation. For the US and Japanese

databases, CFD was performed using STAR-CCM+ (Siemens, Erlangen, Germany) for both mesh generation and CFD simulations. All geometries were converted to computational domains using the same meshing setup: tetrahedral volumetric mesh, minimum element size of 0.1 mm, and 3 refined prism layers. All CFD simulations were performed using the same numeric setup, assumptions, and boundary conditions, including rigid wall, Newtonian behavior of blood flow, location-based inflow rate,<sup>18</sup> and distribution of outlet flow based on the Murray law.<sup>19</sup> Complete details of CFD simulations, including the sensitivity of the hemodynamic results to the CFD solvers, are given in the On-line Appendix and On-line Figs 1 and 2.

### **Morphologic Parameters**

Aneurysmal morphology was calculated using AView,<sup>20-22</sup> a computational workflow for morphologic and hemodynamic assessment of IAs. The definitions of the 13 morphologic indices are illustrated in On-line Fig 3. Maximum diameter (D) is the maximum distance between any 2 points on the aneurysm sac. Maximum height ( $H_{\max}$ ) is the maximum distance between the sac and the center of the neck plane. Height (H) is the maximum perpendicular distance from the neck plane to the sac. Size ratio (SR) has 2 definitions in the literature,<sup>23,24</sup> so does aspect ratio (AR).<sup>23,25</sup> and we applied both.  $SR_D$  is the ratio of D to the average parent vessel diameter, and  $SR_{H_{\max}}$  is the ratio of  $H_{\max}$  to the average parent vessel diameter.  $AR_{H_{\max}}$  and  $AR_H$  are the ratios of  $H_{\max}$  and H to the average neck diameter, respectively. Aneurysm number<sup>26</sup> is the neck ratio (the ratio of neck diameter to the average parent vessel diameter) multiplied by the pulsatility index based on parent artery location obtained from the literature.<sup>27,28</sup> Undulation index (UI) represents the degree of aneurysm surface irregularity. Ellipticity index represents deviation of the IA from a perfect hemisphere. Nonsphericity index represents deviation of the IA from a perfect hemisphere while also considering surface undulations.<sup>23</sup> Surface area and volume of the IAs were calculated as well. We also classified aneurysms as bifurcation or sidewall. Bifurcation IAs are those that arise at the apex of a split from a main (proximal) artery into  $\geq 2$  daughter (distal) arteries.

### **Hemodynamic Parameters**

After obtaining the flow field in each IA, we calculated the aneurysm-averaged values for the following 10 hemodynamic parameters: time-averaged wall shear stress (WSS), which is the WSS magnitude averaged over the aneurysm sac; normalized WSS (NWSS), which is WSS further normalized by the spatiotemporal average wall shear stress of the parent vessel; maximum and minimum WSS and NWSS, which are the maximum or minimum value of WSS that occurred on the aneurysm sac; oscillatory shear index (OSI), which measures the directional change of the WSS through the cardiac cycle; relative residence time (RRT), which quantifies the stasis of blood near the aneurysm wall; low shear area, which is the percentage of the sac area exposed to low WSS (defined as  $<10\%$  of the averaged parent vessel WSS); and finally, complex flow, which is defined as an aneurysmal flow structure that contains  $>1$  separate vortex core line.<sup>18,29</sup> This parameter is

binary: 1 for complex flow structure and 0 for simple flow structure. These parameters are defined in On-line Table 1 and illustrated in On-line Fig 4.

Because multiple operators performed numeric analyses, we conducted a post hoc study to quantify the intraclass correlation coefficient among operators using our protocol for calculating morphologic and hemodynamic parameters and found excellent agreement. Details are provided in the On-line Appendix, On-line Table 2, and On-line Fig 5.

### **Rupture Resemblance Score**

We also calculated the RRS, a rupture classification model that was trained based on a database of 204 ruptured and unruptured IAs.<sup>30</sup> RRS can provide a rupture probability for an IA based on IA morphology and hemodynamics, which can be used to gauge the similarity of an IA to a cohort of ruptured IAs. The equation for the calculation of RRS is provided in the On-line Appendix.

### **Description of Ruptured and Unruptured Aneurysms**

For all IAs, we described location, type (bifurcation versus sidewall), morphology, hemodynamics, and RRS. Continuous variables were presented as means with SDs. Conditional logistic regression<sup>31</sup> was used to assess differences between ruptured and unruptured cohorts. Discrete variables were presented as numbers, and a  $\chi^2$  test was used to determine significant differences between ruptured and unruptured cohorts. A *P* value of  $<.01$  was considered significant.

### **Testing the Performance of Existing Rupture Predictive Parameters in Identifying the Ruptured IA**

We further investigated the performance of each parameter for identifying each patient's ruptured IA. For aneurysm location, rupture prediction was based on rupture site frequencies as reported by Nehls et al<sup>2</sup> (anterior communicating artery, 62% of IAs identified at this location were ruptured; basilar artery, 50%; PICA, 50%; posterior communicating artery, 38%; posterior cerebral artery, 33%; anterior cerebral artery, 33%; ICA, 32%; and MCA, 27%), and the aneurysm with the highest rupture frequency was assumed to be ruptured. If the ruptured IA and a coexisting unruptured IA were located on the same artery or arteries with the same rupture frequency, we assumed that identifying the ruptured aneurysm was not possible, and this was considered a false prediction.

Aneurysm type was used as a predictor of a ruptured aneurysm based on the assumption that bifurcation aneurysms rupture more frequently than sidewall aneurysms, especially small bifurcation aneurysms.<sup>32</sup> Aneurysmal flow pattern was used as a predictor of a ruptured aneurysm based on the assumption that ruptured IAs more frequently contain a complex flow structure.<sup>29</sup> If the ruptured IA and a coexisting unruptured IA were of the same type or had the same flow pattern, we assumed that the rupture site was unidentifiable, and this was considered a false prediction.

For quantitative predictive parameters, the patient's IAs were compared and the IA with the highest value was assumed to be the ruptured IA. For parameters that are generally lower in ruptured aneurysms (eg, NWSS), the aneurysm with the lowest value was assumed to be the ruptured one.



We compared rupture prediction results with actual (confirmed through an operation or definitive hemorrhage pattern) aneurysm rupture status. The performance of each metric was quantified as a positive predictive value, which is the number of patients with correct identification of ruptured IAs divided by the total number of patients.

### Generating Rupture Identification Models

After testing the performance of individual rupture predictors, we generated composite models that were trained to provide a higher score for the ruptured IA in patients with SAH with multiple IAs, which we called the rupture identification model (RIM). First, we randomly assigned 70 patients to a training cohort and 23 patients to a holdout testing cohort. To distribute equal weight, we centered all variables to 0 (subtraction of the mean) and scaled them (division by the SD). All variables were then used to generate all possible linear combinations, and we removed those with collinear variables (Pearson correlation >0.5, moderate correlation; On-line Table 3). We used a linear regression model with a customized cost function, which maximizes the positive predictive value and the differences between ruptured and coexistent unruptured IAs within each patient, to fit the remaining models. The best performing model during 10-fold cross-validation was identified. The resulting model, which was trained by all variables, was termed RIM<sub>C</sub>, with the subscript C indicating the need for CFD to obtain hemodynamic parameters. We also trained a second model by excluding hemodynamic variables, termed RIM<sub>M</sub>, with the subscript M indicating that it is a morphologic parameter and does not require CFD analysis. In the end, we evaluated the final models on the holdout testing cohort as well.

The workflow, access link to the model training code, and additional details of model generation are provided in the On-line Appendix and On-line Fig 6. Statistical analysis and model fitting were performed using an in-house code developed in R statistical and computing software (Version 1.0.44; <https://www.r-project.org/>).

## RESULTS

### Clinical Information

Table 1 summarizes the clinical information of the 93 patients with 206 IAs included in this study: Chinese center (59 patients, 130 IAs), Japanese center (17 patients, 38 IAs), and US center (17 patients, 38 IAs). The average patient age was 60 ± 13 years; 74% of all patients were women. The ruptured aneurysm was identified through craniotomy in 35 patients (38%) and a definitive hemorrhage pattern in 58 patients (62%). Seventy-six patients (82%) had 2 IAs, 15 (16%) had 3 IAs, 1 (1%) had 4 IAs, and 1 (1%) had 5 IAs.

### Description of Ruptured and Unruptured Aneurysms

On-line Table 4 shows the number of IAs at each location, IA type (bifurcation or sidewall), morphology, hemodynamics, and RRS for all IAs in the ruptured and unruptured cohorts. Eighty-two (40%) of all IAs were located along the ICA, 57 (70%) of which were unruptured. The anterior circulation was associated with the highest rupture frequency: Seven of 10 (70%) IAs

**Table 1: Clinical information for patients with SAH with multiple IAs**

Clinical Information	
Demographics and comorbidities (n = 93)	
Age (mean) (yr)	60 ± 13
Female sex	69 (74%)
Hypertension	59 (63%)
Smoking history	35 (38%)
Coronary artery disease	7 (8%)
Hyperlipidemia	28 (30%)
Diabetes mellitus	13 (14%)
Polycystic kidney disease	1 (1%)
Received treatment	
Clipping	35 (38%)
Endovascular	53 (57%)
No treatment	5 (5%)
Aneurysm multiplicity	
2 Aneurysms	76 (82%)
3 Aneurysms	15 (16%)
4 Aneurysms	1 (1%)
5 Aneurysms	1 (1%)

located on the anterior cerebral artery and 16 of 22 (73%) IAs located at the anterior communicating artery were ruptured. Only 6 IAs were located in the posterior circulation. Most ruptured IAs were bifurcation aneurysms (71%).

Except for the nonsphericity index and ellipticity index, the morphologic indices of the ruptured and unruptured cohorts were significantly different. Aneurysmal hemodynamics also differed, with ruptured IAs being exposed to lower WSS, higher RRT, and larger low shear area than the unruptured IAs. Complex flow patterns were present in 62% of ruptured IAs and 20% of unruptured IAs. The RRS was significantly higher in the ruptured cohort ( $P < .001$ ).

### Performance of Existing Parameters in Identifying the Ruptured Aneurysm

All parameters were further analyzed to test their ability in identifying the ruptured aneurysm by calculating the percentage of correctly identified ruptured IAs. We found that the positive predictive value considerably varied by individual parameters from 31% to 87%. SR<sub>Hmax</sub> and H<sub>max</sub> had the highest performance, identifying the ruptured IA in 87% and 85% of patients, respectively (Table 2). RRT identified the ruptured IA in 76% of patients and exhibited the best hemodynamic parameter performance. Figure 2 shows SR<sub>Hmax</sub> and time-averaged RRT distributions on the aneurysm sac for ruptured and unruptured IAs in 3 representative patients. RRS identified the ruptured IA in 80% of the patients.

### Rupture Identification Models

The 2 models, RIM<sub>C</sub> and RIM<sub>M</sub>, tailored to identify the ruptured aneurysm in patients with SAH with multiple IAs, achieved positive predictive values of 93% ± 4% and 90% ± 4%, respectively, during 10-fold cross-validation.

1)

$$RIM_C = 0.45 SR_{Hmax} + 0.17 UI + 0.21 RRT + 0.17 (Bifurcation)$$

**Table 2: Performance of existing aneurysmal parameters in the prediction of ruptured aneurysm in patients with SAH with multiple IAs<sup>a</sup>**

Parameter	Positive Predictive Value
Location	52%
Type	31%
Morphology	
D	82%
H <sub>max</sub>	85%
H	81%
SR <sub>D</sub>	83%
SR <sub>Hmax</sub>	87%
AR <sub>Hmax</sub>	80%
AR <sub>H</sub>	74%
Aneurysm No.	63%
Undulation index	80%
Nonsphericity index	49%
Ellipticity index	40%
Surface area	80%
Volume	80%
Hemodynamics	
WSS	67%
Maximum WSS	55%
Minimum WSS	75%
NWSS	71%
Maximum NWSS	51%
Minimum NWSS	74%
OSI	68%
RRT	76%
LSA	75%
Complex flow	50%
RRS	80%

<sup>a</sup>For WSS, Minimum WSS, NWSS, Maximum NWSS, and Minimum NWSS, we hypothesized that among IAs belonging to each patient, the IA with the lowest value is the ruptured IA. For the rest of the variables, we hypothesized that the IA with the highest value is the ruptured IA.

2)

$$RIM_M = 0.65 \text{ SR}_{Hmax} + 0.16 \text{ UI} + 0.19 (\text{Bifurcation}),$$

where *Bifurcation* equals 1 if an aneurysm is a bifurcation type and 0 if it is a sidewall type.

In the hold-out testing cohort, RIM<sub>C</sub> and RIM<sub>M</sub> could identify the ruptured IA in 92% and 85% of the 23 patients, respectively. Figure 3 shows the performance of RIM<sub>C</sub> and RIM<sub>M</sub> in the 10-fold cross-validation and hold-out testing cohorts.

## DISCUSSION

Identification of the bleeding site is essential to management of aneurysmal SAH because one of the early steps in clinical care is to secure the rupture site to prevent rebleeding. It is often unfeasible to secure all aneurysms discovered in the same setting, so clinicians prioritize treating the highest risk aneurysm first. Misidentification of the ruptured IA may result in disastrous rebleeding of the ruptured lesion and mortality.<sup>2-8</sup> In approximately 50% of patients, the hemorrhage pattern on CT images makes positive identification of the source of bleeding questionable, in which case clinicians often rely on angiographic findings.<sup>2,3</sup> In a study by Orning et al,<sup>3</sup> the ruptured aneurysm was misidentified in 16.2% of patients who had nondefinitive hemorrhage patterns. To create a more reliable aneurysmal metric for identifying the causative lesion, we generated 2 models

(RIM<sub>C</sub> and RIM<sub>M</sub>) that identify the ruptured site in patients with multiple IAs better than existing aneurysmal parameters.

Recent studies have reported using high-resolution MR imaging of the vessel wall for identifying the ruptured aneurysm among multiples.<sup>33,34</sup> However, the reliability of such an approach is not yet established because 28.5% of stable unruptured IAs also demonstrated wall-enhancement features.<sup>35</sup> Moreover, such imaging requires a long acquisition time, which limits its clinical application and requires cooperative or intubated patients.<sup>36</sup> Consequently, the standard of care for identification of ruptured IAs in patients with multiple aneurysms still relies on CT and angiographic findings.

Controversy exists in the literature regarding whether aneurysm size or shape is more reliable for identifying the ruptured IA in patients with multiple IAs. Nehls et al<sup>2</sup> noted that irregular shape, defined as “multilobulated, contained a nipple, or were markedly elongated,” is a better predictor of the ruptured aneurysm than aneurysm size, “greatest dimension.” Conversely, Shojima et al<sup>37</sup> reported that aneurysm size, “largest diameter,” predicts ruptured aneurysms better than irregular shape, which was defined as an aneurysm with a daughter sac or “an irregular protrusion of the aneurysm wall.” We believe such opposing opinions exist because “irregular shape” was not clearly defined and is subject to interrater variations.<sup>22</sup> To avoid such a problem, we quantified aneurysm shape by calculating 3 shape indices, UI, nonsphericity index, and ellipticity index.<sup>23</sup> Among them, UI was the only parameter that was different between ruptured and unruptured IAs, and identified the ruptured IAs in 80% of patients. However, all definitions of aneurysm size, including H<sub>max</sub> and D, outperformed UI in identifying the ruptured IA, indicating that aneurysm size is more reliable than aneurysm shape for ruptured IA identification.

Previous studies have investigated the morphologic and hemodynamic differences between ruptured and unruptured aneurysms in patients with multiple IAs, mainly through regression analysis, which is more suitable for modeling event probabilities.<sup>9,10,12-14,37</sup> In the current study, the ruptured aneurysm was identified by directly comparing the IAs within each patient. We noted that morphology outperformed hemodynamics in identifying ruptured IAs. Among the morphologic parameters that we studied, SR<sub>Hmax</sub> had the highest performance, better than traditional indices such as aneurysm size (D, H<sub>max</sub>) and AR<sub>Hmax</sub>. SR<sub>Hmax</sub> incorporates H<sub>max</sub> and vessel diameter, which is a surrogate for aneurysm location, another variable previously found to be well-correlated with IA rupture.<sup>38</sup>

In a recent study, 17 research groups were asked to use their developed rupture classification models and identify the ruptured aneurysm in a single patient with SAH with 5 IAs. However, only 4 groups could correctly identify the true ruptured aneurysm.<sup>39</sup> In our study, we observed that some individual morphologic parameters, including SR<sub>Hmax</sub> and H<sub>max</sub>, outperformed RRS, a previously developed rupture classification model.<sup>16</sup> This finding indicates that existing rupture classification models, including RRS, may not be tailored to such a specific problem, namely, the identification of the ruptured

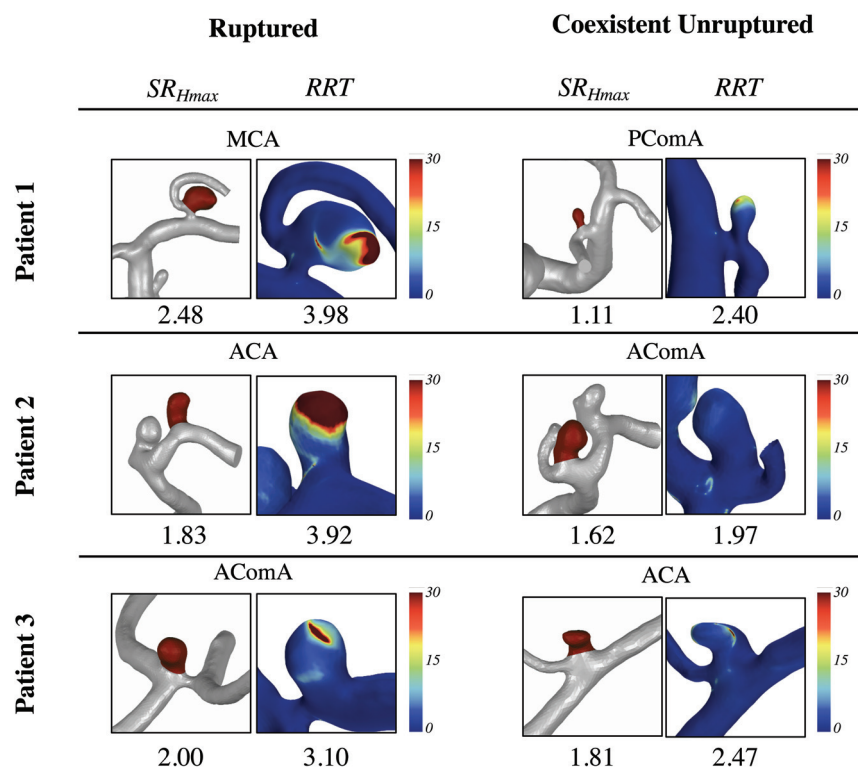


**FIG 2.** Size ratio ( $SR_{Hmax}$ ) and relative residence time for all IAs in 3 representative cases (each patient had 1 ruptured and 1 unruptured IA). The number for the RRT is the spatiotemporal aneurysm averaged over the aneurysm sac.

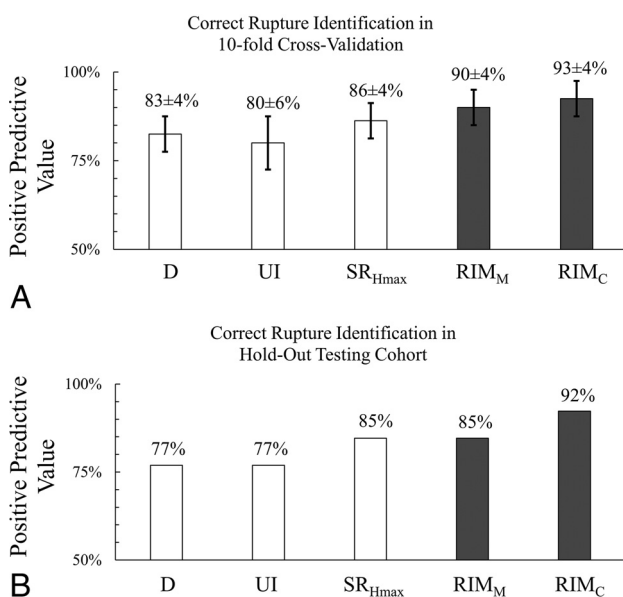


**FIG 3.** Comparison of rupture identification models ( $RIM_C$  and  $RIM_M$ ) with the 3 existing rupture-risk predictors in identifying the ruptured IA in patients with SAH with multiple IAs in 10-fold cross-validation (A) and the holdout testing cohort (B).

IA in patients with multiple IAs. A plausible explanation is that those models were built on the basis of pooled data of individuals with multiple and single IAs. A previous study indicated that the characteristics or natural history of IAs in

patients with multiple aneurysms might be different from those with a single IA.<sup>40</sup> For instance, it was reported that posterior circulation aneurysms were less frequent in patients with multiple IAs than in patients with a single aneurysm, which we also observed in our study (only 3% of IAs were located at the posterior circulation). Moreover, previous models were trained to discriminate ruptured cohorts from unruptured cohorts without associating the coexisting IAs within each patient. Such factors were considered when generating the  $RIM_C$  and  $RIM_M$ . The  $RIM_C$  model incorporated aneurysm  $SR_{Hmax}$ , UI, RRT, and bifurcation type.  $SR_{Hmax}$  and UI represent aneurysm size and shape, respectively, which both are established morphologic metrics for identification of ruptured IAs. RRT is a hemodynamic parameter that incorporates both WSS and OSI. IAs with high RRTs are exposed to high near-wall flow stasis, which could promote inflammatory cell infiltration and aneurysm wall degradation, thereby

increasing the risk of aneurysm rupture.<sup>41</sup> Bifurcation type is a surrogate for locations with high risk of rupture, including the anterior communicating artery, PICA, and posterior communicating artery.<sup>2,42</sup>

As an alternative model that does not require hemodynamic parameters,  $RIM_M$  incorporates only morphologic factors,  $SR_{Hmax}$ , UI, and bifurcation. Although  $RIM_C$  slightly outperformed  $RIM_M$ , we believe that  $RIM_M$  will be more user-friendly in clinical settings by reducing the need for intensive CFD simulations.

Our novel predictive models ( $RIM_M$ ,  $RIM_C$ ) can be helpful in patients with SAH with hemorrhage patterns that are not definitive. In such cases, instead of solely relying on aneurysm size, shape, or location to delineate the ruptured source, the composite rupture identification models may provide more reliable identification.

### Limitations

First, our study had a small sample size and was limited to saccular aneurysms, which could explain the low percentage of posterior circulation aneurysms (3%). Second, definitive hemorrhage patterns were used to identify the rupture source in some of our cases, but only craniotomy can reveal the true rupture status; therefore, there is a possibility of misidentification. Third, our cases came from 3 different centers, and there could be a difference in their aneurysm rupture patterns due to genetics. Fourth, we used several widely used simplifications to perform CFD simulations such as a rigid wall, Newtonian

blood, and generalized boundary conditions to make the computations tractable. Fifth, although we found excellent agreement among users in calculating morphologic and hemodynamic parameters, this was contingent on users following the protocol described in this study. It is unclear how well the rupture identification models will hold if different imaging modalities, segmentation methods, or CFD settings are used. Finally, we used only linear regression models because they were easier to customize for our specific problem. In addition, it was easier to interpret the components (eg, weights) of the final models. In future studies, the application of nonlinear models, such as artificial neural network and random forest, could be explored to account for possible nonlinear interaction among variables.

## CONCLUSIONS

To identify ruptured IAs in patients with SAH with multiple IAs,  $SR_{Hmax}$  is the best predictor among individual morphologic parameters, including location and type, and hemodynamic parameters. However, composite models ( $RIM_C$  and  $RIM_M$ ), specifically designed for identifying the ruptured IA in patients with multiple IAs, outperformed all individual parameters. Between the 2 models,  $RIM_C$ , which incorporated aneurysm hemodynamics, had a better positive predictive value in identifying ruptured IAs, than  $RIM_M$ . These findings may help to improve clinical identification of the ruptured IAs in patients with SAH presenting with multiple aneurysms.

Disclosures: Hui Meng—RELATED: Grant: National Institutes of Health and Canon Medical Systems, Comments: National Institutes of Health grant R01NS091075 R03NS090193, and Canon Medical Systems Corporation grants [no grant number]. Co-founder, Neurovascular Diagnostics, Inc.\* Adnan H. Siddiqui—RELATED: Grant: National Institutes of Health/National Institute of Neurological Disorders and Stroke 1R01NS071075, Virtual Intervention of Intracranial Aneurysms; UNRELATED: Consultancy: Amnis Therapeutics, Boston Scientific, Canon Medical Systems, Cerebrotech Medical Systems, Cerenovus, Corindus, Endostream Medical, Guidepoint Global Consulting, Imperative Care, Integra, Medtronic, MicroVention, Northwest University, Data and Safety Monitoring Board Chair for the HEAT trial, Penumbra, Q'Apel Medical, Rapid Medical, Rebound Therapeutics, Serenity Medical, Silk Road Medical, StimMed, Stryker, Three Rivers Medical, Vassol, W.L. Gore and Associates; Stock/Stock Options: Amnis Therapeutics, BlinkTBI, Buffalo Technology Partners, Cardinal Consultants, Cerebrotech Medical Systems, Cognition Medical, Endostream Medical, Imperative Care, International Medical Distribution Partners, Neurovascular Diagnostics, Q'Apel Medical, Rebound Therapeutics, RIST Neurovascular, Serenity Medical, Silk Road Medical, StimMed, Synchron, Three Rivers Medical, Viseon Spine; Jason M. Davies—RELATED: Grant: National Center for Advancing Translational Sciences of the NIH (award number KL2TR001413), University at Buffalo. Speakers' bureau: Penumbra; Honoraria: Neurotrauma Science; Other: Cerenovus, Medtronic, MicroVention, Penumbra, Medical University of South Carolina, Comments: National Principal Investigator/Steering Committee for Cerenovus LARGE Trial and ARISE II Trial; Medtronic SWIFT PRIME and SWIFT DIRECT trials; MicroVention FRED Trial and CONFIDENCE study; Medical University of South Carolina POSITIVE Trial; Penumbra Separator 3D trial, COMPASS trial, INVEST trial. \*Money paid to the institution.

## ACKNOWLEDGMENTS

We thank Paul H. Dressel, BFA, for figure preparation and W. Fawn Dorr, BA, and Debra J. Zimmer for editorial assistance.

## REFERENCES

- Juvela S. Risk factors for multiple intracranial aneurysms. *Stroke* 2000;31:392–97 [CrossRef Medline](#)
- Nehls DG, Flom RA, Carter LP, et al. Multiple intracranial aneurysms: determining the site of rupture. *J Neurosurg* 1985;63:342–48 [CrossRef Medline](#)
- Orning JL, Shakur SF, Alaraj A, et al. Accuracy in identifying the source of subarachnoid hemorrhage in the setting of multiple intracranial aneurysms. *Neurosurgery* 2018;83:62–68 [CrossRef Medline](#)
- Hino A, Fujimoto M, Iwamoto Y, et al. False localization of rupture site in patients with multiple cerebral aneurysms and subarachnoid hemorrhage. *Neurosurgery* 2000;46:825–30 [CrossRef Medline](#)
- Liu Z, Wei LF, Wang RM, et al. Misdiagnosis of rupture sites of multiple intracranial aneurysms: special report of two cases. *Scientific Research and Essays*, 2010;5:3794–98
- Lee KC, Joo JY, Lee KS. False localization of rupture by computed tomography in bilateral internal carotid artery aneurysms. *Surg Neurol* 1996;45:435–40; discussion 40–41 [CrossRef Medline](#)
- Zderkiewicz E, Pawlik Z, Czocho M, et al. Clinical signs pointing to the source of hemorrhage in multiple intracranial aneurysms. *Med Sci Monit* 2002;8:Cr83–86 [Medline](#)
- Koyama T, Tanaka Y, Kobayashi S, et al. Surgery of basilar aneurysms associated with unexpected rupture of an internal carotid artery aneurysm. *Neurosurg Rev* 2000;23:168–70 [CrossRef Medline](#)
- Bjorkman J, Frosen J, Tahtinen O, et al. Irregular shape identifies ruptured intracranial aneurysm in subarachnoid hemorrhage patients with multiple aneurysms. *Stroke* 2017;48:1986–89 [CrossRef Medline](#)
- Jing L, Fan J, Wang Y, et al. Morphologic and hemodynamic analysis in the patients with multiple intracranial aneurysms: ruptured versus unruptured. *PLoS One* 2015;10:e0132494 [CrossRef Medline](#)
- Doddasomayajula R, Chung B, Mut F, et al. Hemodynamic characteristics of ruptured and unruptured multiple aneurysms at mirror and ipsilateral locations. *AJNR Am J Neuroradiol* 2017;38:2301–07 [CrossRef Medline](#)
- Bhagal P, AlMatter M, Hellstern V, et al. Difference in aneurysm characteristics between ruptured and unruptured aneurysms in patients with multiple intracranial aneurysms. *Surg Neurol Int* 2018;9:1. [CrossRef Medline](#)
- Backes D, Vergouwen MD, Velthuis BK, et al. Difference in aneurysm characteristics between ruptured and unruptured aneurysms in patients with multiple intracranial aneurysms. *Stroke* 2014;45:1299–303 [CrossRef Medline](#)
- Jeon HJ, Lee JW, Kim SY, et al. Morphological parameters related to ruptured aneurysm in the patient with multiple cerebral aneurysms (clinical investigation). *Neurol Res* 2014;36:1056–62 [CrossRef Medline](#)
- Berg P, Beuing O. Multiple intracranial aneurysms: a direct hemodynamic comparison between ruptured and unruptured vessel malformations. *Int J Comput Assist Radiol Surg* 2018;13:83–93 [CrossRef Medline](#)
- Xiang J, Yu J, Choi H, et al. Rupture resemblance score (RRS): toward risk stratification of unruptured intracranial aneurysms using hemodynamic-morphological discriminants. *J Neurointerv Surg* 2015;7:490–95 [CrossRef Medline](#)
- Antiga L, Piccinelli M, Botti L, et al. An image-based modeling framework for patient-specific computational hemodynamics. *Med Biol Eng Comput* 2008;46:1097–12 [CrossRef Medline](#)
- Xiang J, Natarajan SK, Tremmel M, et al. Hemodynamic-morphologic discriminants for intracranial aneurysm rupture. *Stroke* 2011;42:144–52 [CrossRef Medline](#)
- Murray CD. The physiological principle of minimum work, I: the vascular system and the cost of blood volume. *Proc Natl Acad Sci U S A* 1926;12:207–14 [CrossRef Medline](#)
- Rajabzadeh-Oghaz H, Varble N, Davies JM, et al. Computer-assisted adjuncts for aneurysmal morphologic assessment: toward more precise and accurate approaches. *Proc SPIE Int Soc Opt Eng* 2017; 10134 [CrossRef Medline](#)
- Xiang J, Antiga L, Varble N, et al. A View: an image-based clinical computational tool for intracranial aneurysm flow visualization



- and clinical management. *Annals of biomedical engineering*. 2016;44:1085–96 [Medline](#)
22. Rajabzadeh-Oghaz H, Varble N, Shallwani H, et al. Computer-assisted three-dimensional morphology evaluation of intracranial aneurysms. *World Neurosurg* 2018;119:e541–50 [CrossRef Medline](#)
  23. Dhar S, Tremmel M, Mocco J, et al. Morphology parameters for intracranial aneurysm rupture risk assessment. *Neurosurgery* 2008;63:185–97 [CrossRef Medline](#)
  24. Rahman M, Smietana J, Hauck E, et al. Size ratio correlates with intracranial aneurysm rupture status: a prospective study. *Stroke* 2010;41:916–20 [CrossRef Medline](#)
  25. Raghavan ML, Ma B, Harbaugh RE. Quantified aneurysm shape and rupture risk. *J Neurosurg* 2005;102:355–62 [CrossRef Medline](#)
  26. Asgharzadeh H, Borazjani I. Effects of Reynolds and Womersley numbers on the hemodynamics of intracranial aneurysms. *Comput Math Methods Med* 2016;2016:1 [CrossRef Medline](#)
  27. Tsiygoulis G, Sharma VK, Hoover SL, et al. Applications and advantages of power motion-mode Doppler in acute posterior circulation cerebral ischemia. *Stroke* 2008;39:1197–204 [CrossRef Medline](#)
  28. Steinmeier R, Laumer R, Bondar I, et al. Cerebral hemodynamics in subarachnoid hemorrhage evaluated by transcranial Doppler sonography, Part 2: pulsatility indices: normal reference values and characteristics in subarachnoid hemorrhage. *Neurosurgery* 1993;33:10–18 discussion 18–19 [CrossRef Medline](#)
  29. Byrne G, Mut F, Cebal J. Quantifying the large-scale hemodynamics of intracranial aneurysms. *AJNR Am J Neuroradiol* 2014;35:333–38 [CrossRef Medline](#)
  30. Xiang J, Yu J, Snyder KV, et al. Hemodynamic-morphological discriminant models for intracranial aneurysm rupture remain stable with increasing sample size. *J Neurointervent Surg* 2016;8:104–10 [CrossRef Medline](#)
  31. Gail MH, Lubin JH, Rubinstein LV. Likelihood calculations for matched case-control studies and survival studies with tied death times. *Biometrika* 1981;68:703–07 [CrossRef](#)
  32. Feng X, Ji W, Qian Z, et al. Bifurcation location is significantly associated with rupture of small intracranial aneurysms (< 5 mm). *World Neurosurg* 2017;98:538–45 [CrossRef Medline](#)
  33. Matouk CC, Mandell DM, Gunel M, et al. Vessel wall magnetic resonance imaging identifies the site of rupture in patients with multiple intracranial aneurysms: proof of principle. *Neurosurgery* 2013;72:492–96; discussion 496 [CrossRef Medline](#)
  34. Mandell DM, Mossa-Basha M, Qiao Y, et al. Intracranial Vessel Wall MRI: Principles and Expert Consensus Recommendations of the American Society of Neuroradiology. *AJNR Am J Neuroradiol* 2017;38:218–29 [CrossRef Medline](#)
  35. Edjlali M, Gentric JC, Régent-Rodriguez C, et al. Does aneurysmal wall enhancement on vessel wall MRI help to distinguish stable from unstable intracranial aneurysms? *Stroke* 2014;45:3704–06 [CrossRef Medline](#)
  36. Lindenholz A, van der Kolk AG, Zwanenburg JJM, et al. The use and pitfalls of intracranial vessel wall imaging: how we do it. *Radiology* 2018;286:12–28 [CrossRef Medline](#)
  37. Shojima M, Morita A, Nakatomi H, et al. Size is the most important predictor of aneurysm rupture among multiple cerebral aneurysms: post hoc subgroup analysis of Unruptured Cerebral Aneurysm Study Japan. *Neurosurgery* 2018;82:864–69 [CrossRef Medline](#)
  38. Ma D, Tremmel M, Paluch RA, et al. Size ratio for clinical assessment of intracranial aneurysm rupture risk. *Neurol Res* 2010;32:482–86 [CrossRef Medline](#)
  39. Berg P, Voß S, Janiga G, et al. Multiple Aneurysms AnaTomy CHallenge. 2018 (MATCH), Phase II: rupture risk assessment. *Int J Comput Assist Radiology Surg* 2019 May 3. [Epub ahead of print] [CrossRef Medline](#)
  40. Lee YJ, Parreira T, Matouk CC, et al. Clinical characteristics and preferential location of intracranial mirror aneurysms: a comparison with non-mirror multiple and single aneurysms. *Neuroradiology* 2015;57:35–40 [CrossRef Medline](#)
  41. Meng H, Tutino VM, Xiang J, et al. High WSS or low WSS? Complex interactions of hemodynamics with intracranial aneurysm initiation, growth, and rupture: toward a unifying hypothesis. *AJNR Am J Neuroradiol* 2014;35:1254–62 [CrossRef Medline](#)
  42. Varble N, Rajabzadeh-Oghaz H, Wang J, et al. Differences in morphologic and hemodynamic characteristics for “PHASES-Based” intracranial aneurysm locations. *AJNR Am J Neuroradiol* 2017;38:2105–10 [CrossRef Medline](#)